

Co-electrodeposition of Platinum and Rhodium in Poly(3,4-ethylenedioxythiophene)-Poly(styrene sulfonic acid) as Electrocatalyst for Methanol Oxidation

Tzi-Yi Wu¹, Zheng-Yan Kuo², Jiin-Jiang Jow², Chung-Wen Kuo^{2,*}, Cheng-Jang Tsai³,
Pin-Rong Chen¹, Ho-Rei Chen²

¹ Department of Chemical Engineering and Materials Engineering, National Yunlin University of Science and Technology, Yunlin 64002, Taiwan, ROC

² Department of Chemical and Materials Engineering, National Kaohsiung University of Applied Sciences, Kaohsiung 80778, Taiwan, ROC

³ Department of materials Science and Engineering, Far East University, 74448 Tainan, Taiwan

*E-mail: welly@cc.kuas.edu.tw

Received: 18 July 2012 / Accepted: 14 August 2012 / Published: 1 September 2012

Pt and Rh particles are electrochemically loaded into poly(3,4-ethylenedioxythiophene) doped poly(styrene sulfonic acid) matrix by chronocoulometry using the co-deposition technique. X-ray photoelectron spectroscopy (XPS) confirms that the strong interaction between Pt particles and sulfonic acid groups of PEDOT-PSS. X-ray diffraction analysis (XRD) analysis shows a decrease of Pt crystalline facets for the incorporation of Rh into Pt-PEDOT-PSS, indicating a strong interaction between Pt and Rh. The surface morphology of scanning electron microscopy (SEM) analysis reveals a uniform dispersion of Pt/Rh particles in the PEDOT-PSS matrix. Cyclic voltammetry results and chronoamperometric response measurements show that the Pt-Rh-PEDOT-PSS electrode had superior electrocatalytic activity and stability toward methanol oxidation.

Keywords: Poly(3,4-ethylenedioxythiophene)-poly(styrene sulfonic acid), rhodium, cyclic voltammetry, methanol oxidation

1. INTRODUCTION

Direct methanol fuel cells (DMFCs) are considered promising power sources for electric vehicles and electronic portable devices because of their high power density, high vehicle efficiency, relatively quick startup, rapid response to variations in loading, long life, simple system design, and low operating temperature when compared to conventional rechargeable power sources, such as Li ion batteries [1-19]. This is because methanol is a liquid fuel which can be easily stored, handled and

produced from oil, natural gas, coal or biomass [20,21]. However, poor methanol oxidation at the anode and methanol crossover from the anode to cathode remains to be two of the main challenges for the commercial application of DMFC [22]. The negative influence of the methanol crossover can be attenuated by incorporation of methanol-tolerant cathode catalysts, such as platinum-based alloys (PtPb, PtRu, PtAu, PtCo, and PtSn) [23-35]. Recently, many authors have reported improved catalytic performances with these binary catalysts for methanol oxidation. Bimetallic materials have attracted great attention in the field of catalysis and electrocatalysis since the second metal can tailor activities of interest through changes in the chemical, structural, and electronic nature of the particles. However, few reports are available on the catalyst utilization of Pt/Rh bimetallic materials.

In addition, the development of a supporting material is essential to minimize noble metal loadings and achieve optimum catalytic performance. A promising strategy for the development of a supporting material is the introduction of conducting polymers (CPs) [36,37]. CPs, showing interesting optical, electrochemical, and electrical properties are attractive candidates for composite components [38-52]. The CPs can allow a facile flow of electronic charge during the electrochemical oxidation of methanol on Pt. Employ CPs as porous supports can disperse the electrocatalysts and make low-loading catalysts feasible for fuel cell operation [53-58].

Among the CPs that have found favor for use as host matrices for the development of such systems are mainly polyaniline (PANI) [59,60], polypyrrole (PPy) [61,62], and polythiophene (PT) [63] based conducting polymers. Poly(3,4-ethylenedioxythiophene) (PEDOT) and its derivatives appear to be one of the most promising candidates for commercial applications. Poly (3,4-ethylenedioxythiophene) (PEDOT) is an attractive electron conducting polymer. It exhibits high electrical conductivity in its oxidized state with chemical stability under ambient conditions. Moreover, the solubility of PEDOT was enhanced by poly(styrenesulfonate) (PSS) blending. The substitution of carbon by PEDOT or PEDOT-PSS should lead to better catalyst utilization.

Although there are reports about the use of PEDOT-PSS as support for catalytic electrodes in various electrochemical reactions [64], its usage in DMFCs as catalyst support is lacking. The present study is an effort to replace carbon with PEDOT-PSS composite as the catalyst support to realize PEDOT-PSS-supported Pt/Rh electrodes exhibiting mixed conduction within the catalyst layer to help attaining optimum utilization of the Pt catalyst. Pt or Pt-Rh particles were incorporated into PEDOT-PSS film by electrochemical deposition/codeposition from 0.01 M HCl + 0.1 M KCl solution containing (5 mM $\text{H}_2\text{PtCl}_6 \cdot 6\text{H}_2\text{O}$), (5 mM $\text{H}_2\text{PtCl}_6 \cdot 6\text{H}_2\text{O}$ + 1 mM RhCl_3), and (5 mM $\text{H}_2\text{PtCl}_6 \cdot 6\text{H}_2\text{O}$ + 5 mM RhCl_3) for Pt-PEDOT-PSS, Pt-Rh-PEDOT-PSS, and Pt-5Rh-PEDOT-PSS electrodes, respectively. Physicochemical properties of the composites obtained have been characterized by X-ray diffraction (XRD), scanning electron microscopies (SEM), X-ray photoelectron spectroscopy (XPS), and energy-dispersive X-ray (EDX) spectroscopy. It has been demonstrated that Pt-Rh nanoparticles dispersed in PEDOT-PSS matrix can be obtained by a simple procedure when the appropriate preparation conditions are applied. The electrocatalytic activities of these composite catalysts were evaluated by cyclic voltammetry and chronoamperometry methods in 1.0 M methanol + 0.5 M H_2SO_4 solution. It is expected that Pt and Rh particles deposited into the PEDOT-PSS film via electrochemical codeposition to obtain Pt-Rh-PEDOT-PSS and Pt-5Rh-PEDOT-PSS composite electrodes increases the catalyst utilization. Thus, less Pt is used in the modified electrode.

2. EXPERIMENTAL

2.1. Preparation of PEDOT-PSS

PEDOT-PSS (Alfa) matrix electrode was prepared by spin coating (4000 rpm for 20 s) of PEDOT-PSS thin film on the surface of ITO, and then allowed to dry at 150°C for 3 min. A thin film of PEDOT-PSS was formed over a cleaned indium tin oxide (ITO) electrode ($1.0 \times 1.0 \text{ cm}^2$). The regular chemical cleaning procedure of ITO coated glass in an ultrasonic bath used detergent, de-ionized water, and isopropanol in sequence, and then treated by UV-O₃ for 30 min.

2.2. Deposition of Pt, Rh and Pt-Rh particles into PEDOT-PSS matrixes

Pt, Rh, and Pt-Rh particles were incorporated into PEDOT-PSS film by electrochemical deposition/codeposition from 0.01 M HCl + 0.1 M KCl solution containing 5 mM H₂PtCl₆ · 6H₂O (Pt-PEDOT-PSS), 1 mM RhCl₃ (Rh-PEDOT-PSS), 5 mM H₂PtCl₆ · 6H₂O + 1 mM RhCl₃ (Pt-Rh-PEDOT-PSS), 5 mM H₂PtCl₆ · 6H₂O + 5 mM RhCl₃ (Pt-5Rh-PEDOT-PSS) at a constant potential of -0.2 V (vs. Ag/AgCl). For comparison, Pt and Rh particles were also deposited on bare ITO to fabricate E-Pt and E-Rh electrode, respectively. Constant deposition charge of 0.2 C was maintained for all deposition process. After deposition, the electrodes were rinsed with de-ionized water for 5 min and then dried at 150°C for 3 min. The weights of Pt for Pt-PEDOT-PSS Pt-Rh-PEDOT-PSS, and Pt-5Rh-PEDOT-PSS are calculated using XPS, and they are 26, 26 and 36 $\mu\text{g cm}^{-2}$, respectively.

2.3. Physical and electrochemical characterizations

An X-ray photoelectron spectroscopy (XPS) study was performed using an ESCA 210 spectrometer with Mg K α ($h\nu = 1253.6 \text{ eV}$) irradiation as the photon source. The primary tension was 12 kV and the pressure during the scans was approximately 10^{-10} mbar. X-ray diffraction spectra (XRD) for the as-prepared electrodes were obtained by exposing the samples to BRUKER D8 Discover SSS X-ray source with Cu K α ($\lambda = 0.154 \text{ nm}$) as a target in the diffraction angles (2θ) ranged from 10° to 80° with scan rate 4° min⁻¹. The surface morphologies of all electrodes were obtained using a scanning electron microscope (SEM) (JEOL JSM-6700F) equipped with an energy-dispersive X-ray spectroscopy (EDS) detector.

Electrochemical characterizations of Pt-PEDOT-PSS, Pt-Rh-PEDOT-PSS, Pt-5Rh-PEDOT-PSS, and E-Rh composite electrodes were carried out using a CHI627D electrochemical analyzer (U.S.A.). All experiments were performed in a three-component cell. An Ag/AgCl electrode (in 3 M KCl), a Pt wire, and ITO (1-cm^2 area) were used as the reference, counter, and working electrodes, respectively. A Luggin capillary, whose tip was set at a distance of 1-2 mm from the surface of the working electrode, was used to minimize errors due to the iR drop in the electrolytes. An impedance spectrum analyzer was employed to measure and analyze the AC impedance spectra of electrodes obtained at various element resistance values. For the AC signal, the potential amplitude was kept at 10 mV and the frequency range was 1 mHz to 10 kHz.

2.4. Methanol electro-oxidation and stability of Pt-PEDOT-PSS, Pt-Rh-PEDOT-PSS, Pt-5Rh-PEDOT-PSS, and E-Rh composite electrodes

The catalytic activities of Pt-PEDOT-PSS, Pt-Rh-PEDOT-PSS, Pt-5Rh-PEDOT-PSS, and E-Rh composite electrodes were examined by cyclic voltammetry (CV) at 10 mV sec^{-1} in the range of -0.2 to 1.2 V. Chronoamperometric response curves were obtained at 0.6 V in 1.0 M CH_3OH + 0.5 M H_2SO_4 solution. All the electrochemical experiments were carried out at room temperature.

3. RESULTS AND DISCUSSION

3.1. XPS analysis

XPS study was employed to analyze the binding energy related to S_{2p} core-level spectra of PEDOT-PSS, Pt-PEDOT-PSS, Pt-Rh-PEDOT-PSS, and Pt-5Rh-PEDOT-PSS. The sulfur core level spectrum of PEDOT-PSS film coated on ITO is shown in curve (a) of Fig. 1. The curve shows large differences in binding energy depending on the S location of PEDOT and PSS. The peak at 168.5 eV corresponds to spin-orbit splitting doublet originates from the sulfur atom of PSS dopants. However, the spin-orbit splitting doublet of PEDOT sulfur originates at 164.5 eV. These observations were similar to the binding energy of S_{2p} core level spectra of PEDOT-PSS film obtained by sputtering on ITO [65]. After the addition of Pt or Pt-Rh particles on PEDOT-PSS film, significant changes occurred in S_{2p} core value of sulfur in both PEDOT and PSS. The curve b, c, and d show the formation of a shoulder peak (C-S-Pt binding energy) at 161.0~161.8 eV. This evaluation is a good agreement for typical C-S-metal bonds appearing in the range between 162 eV and 161 eV [66]. Jonsson *et al.* [67] reported that aluminum/PEDOT-PSS contains an interfacial layer formed by chemical interactions between aluminum and mainly sulfonic groups of poly(styrenesulfonic acid) (PSS). The sulfur atoms of PSS might be bonded with Pt atoms more easily than that of PEDOT. This is due to the fact that the PEDOT doped with excess PSS can react easily with Pt particle surface. From the analysis of S elements, we concluded that the strong interaction between Pt particles and sulfonic acid groups of PEDOT-PSS.

3.2. Structural characterization of composite electrodes

The surface morphology of Pt or Pt-Rh particles incorporated in PEDOT-PSS electrode was examined by XRD analysis and shown in Fig. 2. The characteristic diffraction peaks of bare ITO was observed at about 31° , 36° , 51° , and 61° , corresponding to (222), (400), (440), and (622) plane, respectively. The XRD pattern of Pt-PEDOT-PSS obtained using similar fabricating method is also shown in curve b. The characteristic diffraction peaks of face centered cubic (fcc) platinum were observed at 39.9° , 46.5° , and 68.0° correspond to Pt (111), (200), and (220) plane, respectively. E-Rh electrode presented reflection peaks at about 41.1° , 47.8° , and 69.6° , which was assigned to rhodium metal particles (curve e) [68]. The diffraction peaks of Rh were found difficulty from XRD pattern of

Pt-Rh-PEDOT-PSS and Pt-5Rh-PEDOT-PSS (curve c and d) due to low amounts of Rh particles [24]. But co-deposition of Pt/Rh particles onto PEDOT-PSS film, the diffraction peak values of Pt (111) and Pt (200) facets are shifted to higher values compared to the respective Pt facets in the bare ITO (curve a). The Pt (111) and Pt (200) facets of Pt-Rh-PEDOT-PSS and Pt-5Rh-PEDOT-PSS become broader than Pt-PEDOT-PSS, which indicate that the dispersing nature of Pt particles with less particles aggregation in PEDOT-PSS matrix. This observation is clearly seen in inset of Fig. 2. The reduced peak intensity of Pt (111) and Pt (200) facets was also observed for both Pt-Rh-PEDOT-PSS and Pt-5Rh-PEDOT-PSS, indicating that the crystalline lattice of platinum might be influenced by the existence of Rh particles in composite systems and the strong interaction between Pt and Rh.

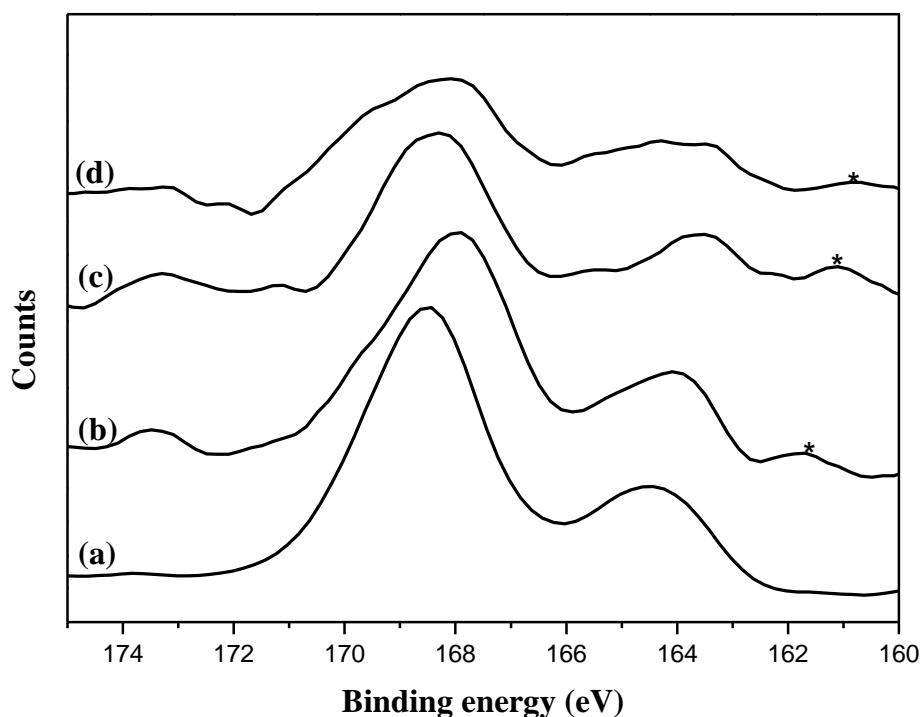


Figure 1. S_{2p} XPS core-level spectra of (a) PEDOT-PSS, (b) Pt-PEDOT-PSS, (c) Pt-Rh-PEDOT-PSS, and (d) Pt-5Rh-PEDOT-PSS.

3.3. Surface morphology of Pt or Pt-Rh particles in PEDOT-PSS film

Fig. 3a-d shows the scanning electron microscopy (SEM) analysis of surface morphology of E-Pt, Pt-PEDOT-PSS, Pt-Rh-PEDOT-PSS, and Pt-5Rh-PEDOT-PSS electrodes. The aggregation of Pt particles was clearly seen on bare ITO for simple deposition of Pt (Fig. 3a), whereas smaller particles size of Pt (100-300 nm) with high active surface area was observed for Pt-PEDOT-PSS electrode compared to E-Pt. Since PEDOT-PSS act as 3D-random matrix, SO_3^- groups of PEDOT-PSS uptake of Pt^{4+} ions and a protective layer to prevent the aggregation of Pt particles after Pt formation. The S_{2p} core level spectra of XPS showed that the PEDOT-PSS-Pt electrode has the strong interaction between platinum and sulfonic groups of PEDOT-PSS. Moreover, homogeneous distribution of Pt-Rh particles are clearly shown in Pt-Rh-PEDOT-PSS matrix with average particles size about 50-200 nm by co-deposition of metal precursor salt solution using chronocoulometry technique. In contrast to Pt-

PEDOT-PSS, less aggregation of Pt particles can be observed for Pt-Rh-PEDOT-PSS and Pt-5Rh-PEDOT-PSS. The possible explanation is that the addition of Rh might inhibit the agglomeration of Pt particles. The existence of Rh can not be seen for all composite electrodes from SEM images. Hence, the EDS plot confirms the existence of Pt and Rh in the PEDOT-PSS film (Fig. 4). As shown in Table 1, the Pt-5Rh-PEDOT-PSS electrode contains more Rh atoms than that of Pt-Rh-PEDOT-PSS due to the existence of larger amounts of Rh.

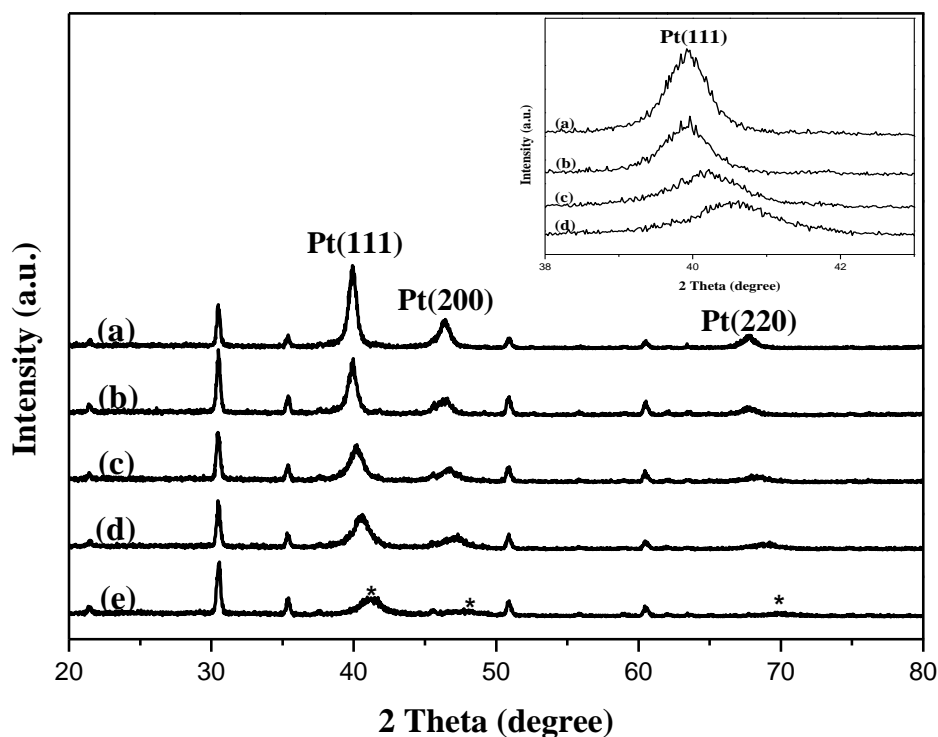


Figure 2. XRD patterns of (a) E-Pt, (b) Pt-PEDOT-PSS, (c) Pt-Rh-PEDOT-PSS, (d) Pt-5Rh-PEDOT-PSS, and (e) E-Rh.

3.4. Electrocatalytic activity of Pt or Pt-Rh particles loaded into PEDOT-PSS film

Pt or Pt-Rh particles were loaded into PEDOT-PSS composite electrodes and tested for their electrocatalytic activity of methanol oxidation by cyclic voltammetry. Fig. 5 shows voltammograms of Pt-PEDOT-PSS, Pt-Rh-PEDOT-PSS, Pt-5Rh-PEDOT-PSS, and E-Rh composite electrodes obtained in 0.5 M H_2SO_4 solution containing 1.0 M methanol at a scan rate of 10 mV s^{-1} . Comparing the CV results of the electrodes, a significantly higher oxidation current toward methanol oxidation was observed for Pt-Rh-PEDOT-PSS compared to those of the other electrodes. A maximum anodic peak current density of $185 \text{ mA cm}^{-2} \text{ mg}^{-1}$ was observed for the Pt-Rh-PEDOT-PSS electrode (that for Pt-PEDOT-PSS was $175 \text{ mA cm}^{-2} \text{ mg}^{-1}$). The voltammograms of the E-Rh electrode show no characteristic methanol oxidation peak, indicating that E-Rh particles are electro-catalytically inactive toward methanol oxidation (inset, Fig. 5d). The enhanced catalytic activity of Pt-Rh-PEDOT-PSS toward methanol oxidation is thus attributed to the facile oxidation of methanol by Rh particles in Pt-

PEDOT-PSS. However, the oxidation current density for methanol oxidation is about $50 \text{ mA cm}^{-2} \text{ mg}^{-1}$ for Pt-5Rh-PEDOT-PSS, which is lower than that of Pt-Rh-PEDOT-PSS. This might be due to an excessive number of Rh particles cover the surface of Pt particles. In addition, the onset of methanol oxidation occurs at about 0.43, 0.37, and 0.38 V for Pt-PEDOT-PSS, Pt-Rh-PEDOT-PSS, and Pt-5Rh-PEDOT-PSS, respectively.

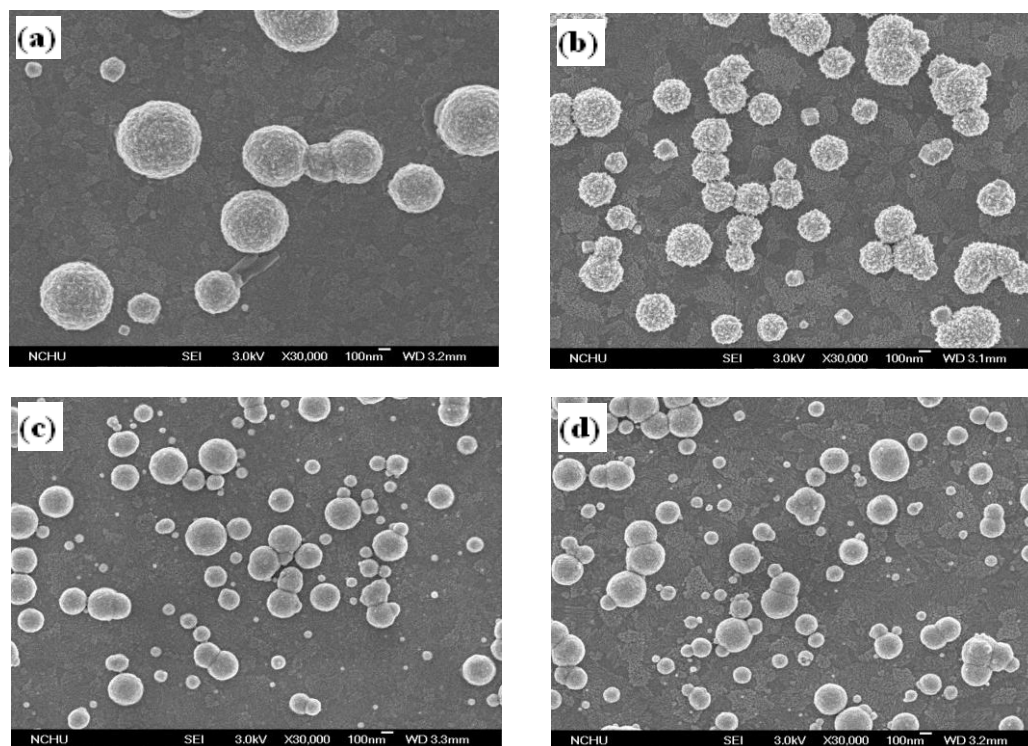


Figure 3. SEM images of (a) E-Pt, (b) Pt-PEDOT-PSS, (c) Pt-Rh-PEDOT-PSS, and (d) Pt-5Rh-PEDOT-PSS.

Table 1. Atomic percentage of each element in Pt-PEDOT-PSS, Pt-Rh-PEDOT-PSS, and Pt-5Rh-PEDOT-PSS electrodes from XPS analysis.

| Electrode | C | O | Cl | S | Rh | Pt |
|------------------|------|------|------|-----|-----|------|
| Pt-PEDOT-PSS | 50.8 | 29.8 | 8.2 | 3.9 | 0.0 | 7.3 |
| Pt-Rh-PEDOT-PSS | 53.8 | 19.2 | 10.9 | 2.1 | 2.0 | 12.0 |
| Pt-5Rh-PEDOT-PSS | 48.1 | 22.4 | 14.8 | 1.7 | 5.5 | 7.5 |

The low onset of methanol oxidation observed in this study is due to less CO poisoning of Pt particles as a result of the fast reaction between Rh particles and the Pt-CO intermediate during methanol oxidation. Furthermore, the ratio of the forward oxidation current peak (I_f) to the reverse current peak (I_b), I_f/I_b , is an important index of the catalyst tolerance to the carbonaceous species

accumulation, Pt-CO [69]. As shown in Table 2, the I_f/I_b value is calculated to be 18.5 for Pt-Rh-PEDOT-PSS and 1.7 for Pt-PEDOT-PSS, respectively, whereas the I_b value of the Pt-5Rh-PEDOT-PSS electrode is difficult to evaluate from observation. The high I_f/I_b value for Pt-Rh-PEDOT-PSS indicates that more effective oxidation of methanol occurs and most of the intermediate carbonaceous species have been oxidized to CO_2 during the forward potential scan.

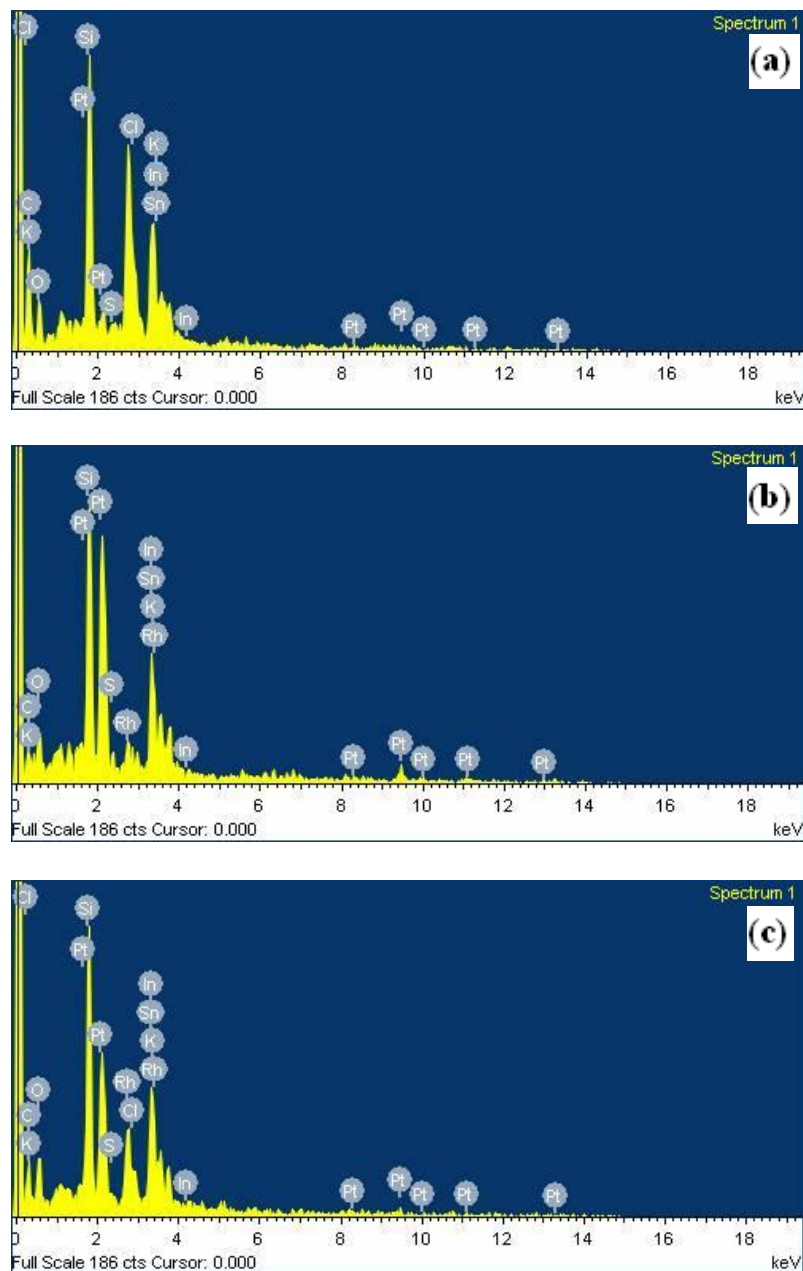


Figure 4. EDS plots for (a) Pt-PEDOT-PSS, (b) Pt-Rh-PEDOT-PSS, (c) Pt-5Rh-PEDOT-PSS.

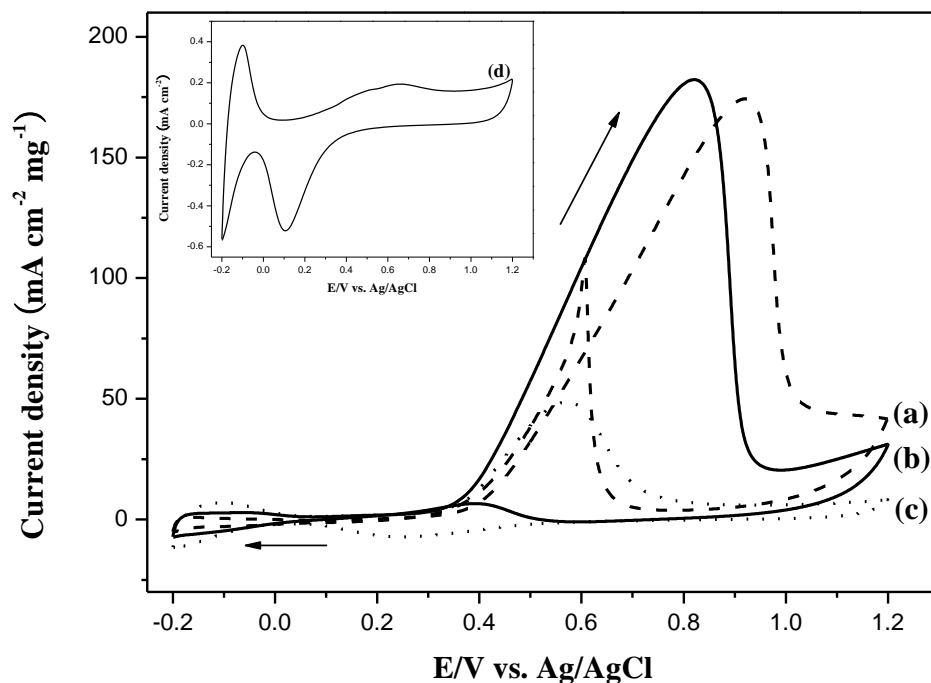
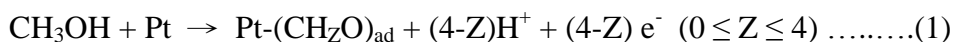


Figure 5. Cyclic voltammograms of (a) Pt-PEDOT-PSS, (b) Pt-Rh-PEDOT-PSS, (c) Pt-5Rh-PEDOT-PSS, and (d) E-Rh (inset) in 1.0 M CH₃OH + 0.5 M H₂SO₄ solution with a scanning rate of 10 mV s⁻¹.

Table 2. Cyclic voltammetric data for Pt-PEDOT-PSS, Pt-Rh-PEDOT-PSS, and Pt-5Rh-PEDOT-PSS electrodes.

| Electrode | Onset / V | I _f / mA cm ⁻² mg ⁻¹ | I _b / mA cm ⁻² mg ⁻¹ | I _f / I _b |
|------------------|-----------|---|---|---------------------------------|
| Pt-PEDOT-PSS | 0.43 | 175 | 105 | 1.7 |
| Pt-Rh-PEDOT-PSS | 0.37 | 185 | 10 | 18.5 |
| Pt-5Rh-PEDOT-PSS | 0.38 | 50 | — | — |

Based on the above supposition, the following mechanism is proposed for the oxidation of methanol in 0.5 M H₂SO₄ at the Pt-Rh-PEDOT-PSS electrode by the dissociative adsorption process. This results in a series of adsorbed intermediates forming on the Pt surface [70].



The role of Rh particles in Pt-Rh catalysts for methanol oxidation is considered to be similar to that of ruthenium in platinum-ruthenium catalysts, in which species on ruthenium can oxidize the adsorption of CO on platinum. The Rh helps the transformation of adsorbed intermediates to carbon dioxide. The clean Pt surface then becomes available for further oxidation of methanol.

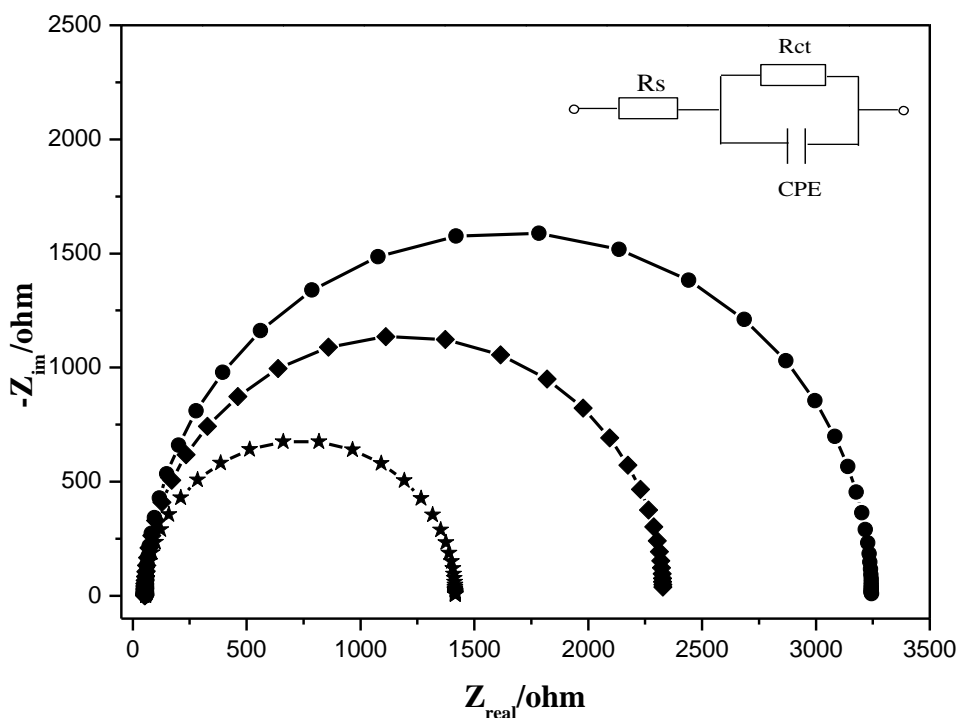
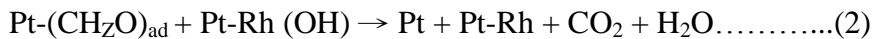


Figure 6. Nyquist plots for Pt-PEDOT-PSS (●), Pt-5Rh-PEDOT-PSS (◆), and Pt-Rh-PEDOT-PSS (★) electrodes in 1.0 M CH₃OH + 0.5 M H₂SO₄ solution and an applied potential of 0.40 V vs. Ag/AgCl using a AC amplitude of 10.0 mV. Equivalent circuit was used to fit the impedance spectra (inset).

3.5. Electrochemical impedance spectroscopy measurements

Mechanism for oxidation of methanol confirmed by electrochemical impedance spectroscopy (EIS) measurements. The EIS was used to determine the charge-transfer resistance for Pt-PEDOT-PSS, Pt-5Rh-PEDOT-PSS, and Pt-Rh-PEDOT-PSS toward methanol oxidation. Fig. 6 shows the Nyquist plots obtained in 1.0 M CH₃OH + 0.5 M H₂SO₄ solution at applied potential of 0.40 V vs. Ag/AgCl using a AC amplitude of 10.0 mV for Pt-PEDOT-PSS, Pt-5Rh-PEDOT-PSS, and Pt-Rh-PEDOT-PSS electrodes. At the potential of 0.40 V vs. Ag/AgCl, the CO is absorbed on the surface of platinum particles during the methanol oxidation process and Rh can oxidize CO surface of platinum particles. To interpret the impedance results, the equivalent circuit was used to fit the EIS data in Fig. 6 (inset). This circuit consists of a solution resistance (R_s) in series with a parallel combination of charge transfer resistance (R_{ct}) and constant phase element (CPE), the parallel combination (R_{ct} and CPE) leads to a depressed semicircle in the corresponding Nyquist impedance plot.

According to experiment data based on equivalent circuits, it is clear that the lowest charge-transfer resistance (R_{ct} = 1.35 kΩ) can be observed for Pt-Rh-PEDOT-PSS than Pt-PEDOT-PSS (R_{ct} = 3.18 kΩ) due to the presence of Rh in Pt-PEDOT-PSS matrix. This can be explained by Rh oxidized

CO of platinum surface to form CO_2 . Moreover, the charge-transfer resistance of Pt-Rh-PEDOT-PSS is lower than that of Pt-5Rh-PEDOT-PSS ($R_{ct} = 2.27 \text{ k}\Omega$), implying excess Rh particles on Pt-PEDOT-PSS electrode causes higher charge-transfer resistance.

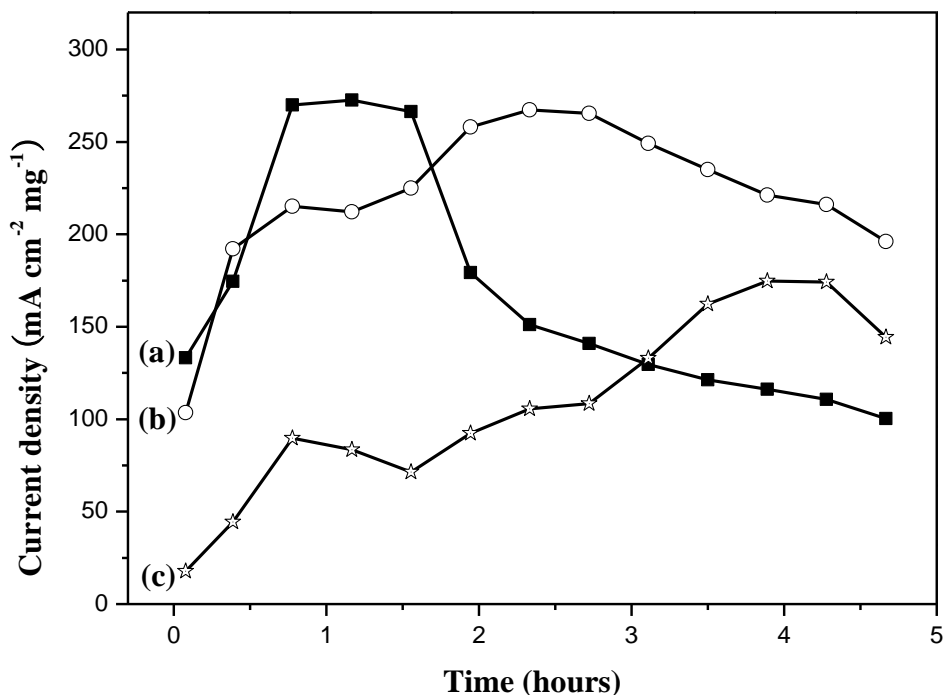


Figure 7. Long-term stability of (a) Pt-PEDOT-PSS, (b) Pt-Rh-PEDOT-PSS, and (c) Pt-5Rh-PEDOT-PSS in 1.0 M CH_3OH + 0.5 M H_2SO_4 aqueous solution. Note: Experiment was carried out using cyclic voltammetry from -0.2 to 1.2 V at a scan rate of 10 mVs^{-1} for 60 cycles (4.7 h), operating time was estimated from cycle numbers.

3.6. Electrocatalytic long-time stability of Pt or Pt-Rh particles loaded into PEDOT-PSS film

The long-term stability of Pt-PEDOT-PSS, Pt-Rh-PEDOT-PSS, and Pt-5Rh-PEDOT-PSS for methanol oxidation were examined in 1.0 M CH_3OH + 0.5 M H_2SO_4 solution at a 10 mVs^{-1} scanning rate for 60 cycles (4.7 h). The scan rate employed in the work allows CO to form at 0.4 V. We anticipate that the formation of CO and adsorption on Pt sites become significant with increasing cycle numbers for methanol oxidation. The drop of the maximum current is attributed to the CO poisoning of Pt active sites during the scanning in aqueous solution. The overall electrocatalytic performance of the test electrodes will be affected by deactivation due to the CO poisoning on Pt active sites. The plot of forward oxidation current peak (I_f) for methanol oxidation vs. time (estimated from cycle numbers) is presented in Fig. 7. It shows that anodic current increases with increasing operation time at the initial stage for all the electrodes. After long-time, the anodic currents of methanol oxidation for all the electrodes first reach a maximum and then decrease. The decrease in the anodic current for methanol oxidation can be attributed to the poisoning of active Pt sites by CO species produced during methanol oxidation. Interestingly, Pt-Rh-PEDOT-PSS and Pt-5Rh-PEDOT-PSS exhibited different

characteristics from that of Pt-PEDOT-PSS. The current increases after a slight fall, implying that the active Pt sites might be regenerated during this period. However, the oxidation current density for methanol oxidation for Pt-Rh-PEDOT-PSS is higher than that of Pt-5Rh-PEDOT-PSS for 60 cycles, this might be due to an excessive amounts of Rh particles cover the surface of Pt particles.

Additionally, the performance of Pt-5Rh-PEDOT-PSS, Pt-PEDOT-PSS, and Pt-Rh-PEDOT-PSS electrodes towards the methanol oxidation reaction after long-time operation was tested using chronoamperometry. Fig. 8 shows the chronoamperograms of Pt-5Rh-PEDOT-PSS, Pt-PEDOT-PSS, and Pt-Rh-PEDOT-PSS electrodes recorded at 0.6 V in solution of 1.0 M CH₃OH + 0.5 M H₂SO₄ for 3 hours. After long-time operation, a steady state current density is achieved. It can be observed that Pt-Rh-PEDOT-PSS electrocatalyst maintained the highest current density. For example, the currents at 2.5 h are 10.5, 6.0, and 2.0 mA cm⁻² mg⁻¹ for Pt-Rh-PEDOT-PSS, Pt-PEDOT-PSS, and Pt-5Rh-PEDOT-PSS electrodes, respectively.

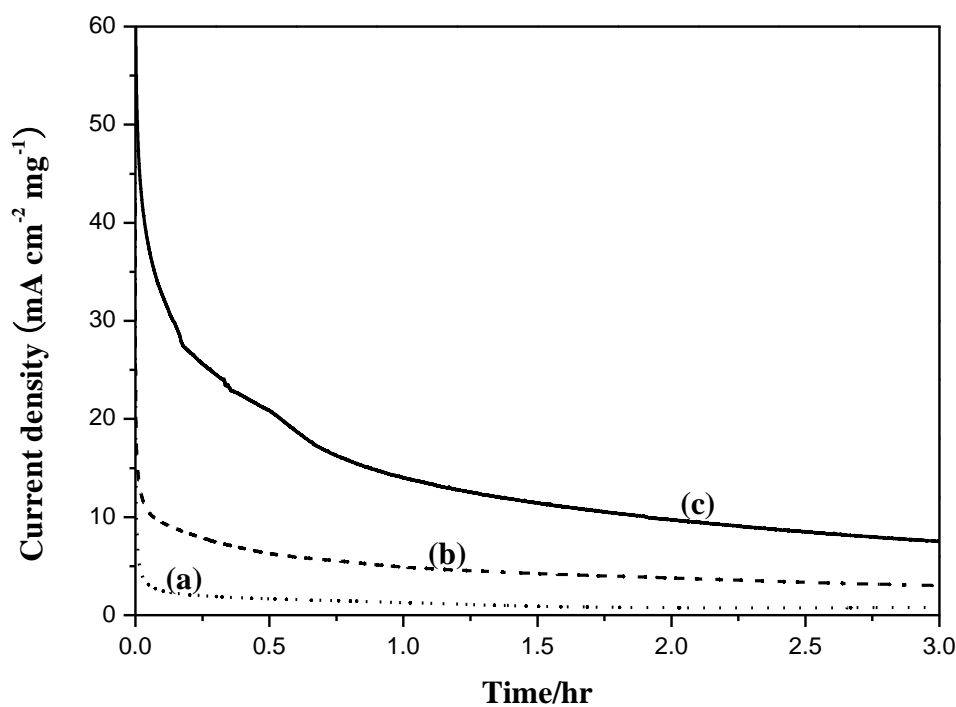


Figure 8. Chronoamperometric responses of (a) Pt-5Rh-PEDOT-PSS, (b) Pt-PEDOT-PSS, and (c) Pt-Rh-PEDOT-PSS at 0.6 V (vs. Ag/AgCl) in 1.0 M CH₃OH + 0.5 M H₂SO₄ solution.

4. CONCLUSIONS

Pt and Rh particles were successfully embedded into PEDOT-PSS matrix to form Pt-Rh-PEDOT-PSS composite electrode by electrochemical codeposition. The Pt-Rh-PEDOT-PSS based composite electrode exhibits a higher current density and stability toward methanol oxidation, demonstrating Pt-Rh-PEDOT-PSS electrode is a promising material as catalysts for methanol oxidation. The -SO₃H group in polymer matrix for 3D deposition of Pt and Rh is interesting and the Rh

favors the transformation of CO to carbon dioxide on platinum surface. PEDOT-PSS matrix provides an environment for dispersing Pt and Rh particles with less aggregation, and PEDOT-PSS matrix is a potential candidate for preparing anode electrocatalyst in direct methanol fuel cell.

ACKNOWLEDGEMENTS

The financial support of this work by the National Science Council of Taiwan under NSC 101-2221-E-151-058, NSC 99-2218-E-151-003, and NSC101-2218-E-224-002 are gratefully acknowledged.

References

1. B.C.H. Steele, A. Heinzl, *Nature*, 414 (2001) 345.
2. J. Gao, J. Liu, W. Liu, B. Li, Y. Xin, Y. Yin, Z. Zou, *Int. J. Electrochem. Sci.*, 6 (2011) 6115.
3. M.S. Mohy Eldin, M.A. Abu-Saied, A.A. Elzatahry, K.M. El-Khatib, E.A. Hassan, M.M. El-Sabbah, *Int. J. Electrochem. Sci.*, 6 (2011) 5417.
4. H.D. Herrera-Méndez, P. Roquero, M.A. Smit, L.C. Ordóñez, *Int. J. Electrochem. Sci.*, 6 (2011) 4454.
5. R.S. Amin, A.A. Elzatahry, K.M. El-Khatib, M. Elsayed Youssef, *Int. J. Electrochem. Sci.*, 6 (2011) 4572.
6. H. Zhang, G. Lin, J. Chen, *Int. J. Electrochem. Sci.*, 6 (2011) 4714.
7. C. Guzmán, A. Alvarez, J. Ledesma-García, S.M. Duron-Torres, L.G. Arriaga, *Int. J. Electrochem. Sci.*, 6 (2011) 4787.
8. Y. Li, S.M. Chen, R. Sarawathi, *Int. J. Electrochem. Sci.*, 6 (2011) 3776.
9. J.H. Kim, S.K. Kim, Y.Z. You, D.I. Kim, S.T. Hong, H.C. Suh, K.S. Weil, *Int. J. Electrochem. Sci.*, 6 (2011) 4365.
10. A. Rezazadeh, A. Askarzadeh, M. Sedighzadeh, *Int. J. Electrochem. Sci.*, 6 (2011) 3105.
11. S. Garbarino, L.D. Burke, *Int. J. Electrochem. Sci.*, 5 (2010) 828.
12. D.C. Huang, P.J. Yu, F.J. Liu, S.L. Huang, K.L. Hsueh, Y.C. Chen, C.H. Wu, W.C. Chang, F.H. Tsau, *Int. J. Electrochem. Sci.*, 6 (2011) 2551.
13. J.P. Spets, M.J. Lampinen, Y. Kiros, T. Anttila, J. Rantanen, T. Granström, *Int. J. Electrochem. Sci.*, 5 (2010) 547.
14. M. ElSayed Youssef, K.E. AL-NAdi, M.H. Khalil, *Int. J. Electrochem. Sci.*, 5 (2010) 267.
15. M.B. Rodríguez, M.G.A.R. Paleta, J.A.R. Márquez, J.R.G. de la Vega, *Int. J. Electrochem. Sci.*, 5 (2010) 414.
16. J.H. Myung, H.J. Ko, J.J. Lee, S.H. Hyun, *Int. J. Electrochem. Sci.*, 6 (2011) 1617.
17. C.M. Bautista-Rodríguez, M.G.A. Rosas-Paleta, J.A. Rivera-Marquez, N. Tepale-Ochoa, *Int. J. Electrochem. Sci.*, 6 (2011) 256.
18. A. Suzuki, T. Hattori, R. Miura, H. Tsuboi, N. Hatakeyama, H. Takaba, M.C. Williams, A. Miyamoto, *Int. J. Electrochem. Sci.*, 5 (2010) 1948.
19. W.H. Chen, T.H. Ko, J.H. Lin, C.H. Liu, C.W. Shen, C.H. Wang, *Int. J. Electrochem. Sci.*, 6 (2011) 2192.
20. A. Anis, S.M. Al-Zahrani, A.K. Banthia, S. Bandyopadhyay, *Int. J. Electrochem. Sci.*, 6 (2011) 2461.
21. A. Anis, S.M. Al-Zahrani, A.K. Banthia, S. Bandyopadhyay, *Int. J. Electrochem. Sci.*, 6 (2011) 2652.
22. R. Awasthi, R.N. Singh, *Int. J. Electrochem. Sci.*, 6 (2011) 4775.
23. R.M.S. Rodrigues, R.R. Dias, C.A.L.G.O. Forbicini, M. Linardi, E.V. Spinacé, A.O. Neto, *Int. J. Electrochem. Sci.*, 6 (2011) 5759.
24. G.S. Buzzo, M.J.B. Orlandi, E. Teixeira-Neto, H.B. Suffredini, *Int. J. Electrochem. Sci.*, 6 (2011) 3768.

25. D.F. da Silva, A.N. Geraldes, E.Z. Cardoso, M.M. Tusi, M. Linardi, E.V. Spinacé, A.O. Neto, *Int. J. Electrochem. Sci.*, 6 (2011) 3594.
26. D. Morales-Acosta, D. López de la Fuente, L.G. Arriaga, G. Vargas Gutiérrez, F. J. Rodríguez Varela, *Int. J. Electrochem. Sci.*, 6 (2011) 1835.
27. R.M. Piasentin, E.V. Spinacé, M.M. Tusi, A.O. Neto, *Int. J. Electrochem. Sci.*, 6 (2011) 2255.
28. H. Li, D. Kang, H. Wang, R. Wang, *Int. J. Electrochem. Sci.*, 6 (2011) 1058.
29. C.H. Wan, J.M. Wei, M.T. Lin, C.H. Lin, *Int. J. Electrochem. Sci.*, 6 (2011) 889.
30. A.B. Kashyout, A.A. Nassr Abu Bakr, L. Giorgi, T. Maiyalagan, B.A.B. Youssef, *Int. J. Electrochem. Sci.*, 6 (2011) 379.
31. M. Brandalise, M.M. Tusi, R.M.S. Rodrigues, E.V. Spinace, A.O. Neto, *Int. J. Electrochem. Sci.*, 5 (2010) 1879.
32. R.F.B. De Souza, M.M. Tusi, M. Brandalise, R.R. Dias, M. Linardi, E.V. Spinace, M.C. dos Santos, A.O. Neto, *Int. J. Electrochem. Sci.*, 5 (2010) 895.
33. M. Brandalise, M.M. Tusi, R.M. Piasentin, M. Linardi, E.V. Spinace, A.O. Neto, *Int. J. Electrochem. Sci.*, 5 (2010) 39.
34. J. Parrondo, R. Santhanam, F. Mijangos, B. Rambabu, *Int. J. Electrochem. Sci.*, 5 (2010) 1342.
35. X.J. Feng, Y.L. Shi, Z.A. Hu, *Int. J. Electrochem. Sci.*, 5 (2010) 489.
36. H.H. Zhou, S.Q. Jiao, J.H. Chen, W.Z. Wei, Y.F. Kuang, *J. Appl. Electrochem.*, 34 (2004) 455.
37. C.C. Yang, T.Y. Wu, H.R. Chen, T.H. Hsieh, K.S. Ho, C.W. Kuo, *Int. J. Electrochem. Sci.*, 6 (2011) 1642.
38. C.W. Kuo, C. Sivakumar, T.C. Wen, *J. Power Sources*, 185 (2008) 807.
39. T.Y. Wu, R.B. Sheu, Y. Chen, *Macromolecules*, 37 (2004) 725.
40. C.W. Kuo, T.C. Wen, *Eur. Polym. J.*, 44 (2008) 3393.
41. T.Y. Wu, Y. Chen, *J. Polym. Sci. A Polym. Chem.*, 42 (2004) 1272.
42. Y. Chen, T.Y. Wu, *Polymer*, 42 (2001) 9895.
43. X.H. Zhu, L.Y. Xu, M. Wang, Z. Wang, R.M. Liu, J.S. Zhao, *Int. J. Electrochem. Sci.*, 6 (2011) 1730.
44. T.Y. Wu, Y. Chen, *J. Polym. Sci.: Part A: Polym. Chem.*, 40 (2002) 3847.
45. Q.X. Wang, X.L. Wang, Z.L. Yu, X.L. Yuan, K. Jiao, *Int. J. Electrochem. Sci.*, 6 (2011) 5470.
46. T.Y. Wu, Y. Chen, *J. Polym. Sci.: Part A: Polym. Chem.*, 40 (2002) 4570.
47. A.C. de Sa, L.L. Paim, U.D. Bicalho, D.R. do Carmo, *Int. J. Electrochem. Sci.*, 6 (2011) 3754.
48. T.Y. Wu, Y. Chen, *J. Polym. Sci.: Part A: Polym. Chem.*, 40 (2002) 4452.
49. R.A. Olowu, A. Williams, P.M. Ndagili, R.F. Ngece, S.N. Mailu, P. Baker, E. Iwuoha, *Int. J. Electrochem. Sci.*, 6 (2011) 1855.
50. T.Y. Wu, Y. Chen, *J. Polym. Sci.: Part A: Polym. Chem.*, 41 (2003) 1444.
51. D.P. dos Santos, M.F. Bergamini, M.V.B. Zanoni, *Int. J. Electrochem. Sci.*, 5 (2010) 1399.
52. T.Y. Wu, N.C. Lee, Y. Chen, *Synth. Met.*, 139 (2003) 263.
53. C.W. Kuo, Z.Y. Kuo, J.J. Jow, T.Y. Wu, J.Y. Chen, X.X. Zhu, *Int. J. Electrochem. Sci.*, 7 (2012) 4974.
54. C.W. Kuo, P.L. Kuo, K.S. Ho, T.H. Hsieh, S.J. Chen, T.Y. Wu, Y.C. Huang, *J. Chin. Chem. Soc.*, 2012, in press, doi: 10.1002/jccs.201200090.
55. C.W. Kuo, L.M. Huang, T.C. Wen, A. Gopalan, *J. Power Sources*, 160 (2006) 65.
56. L.M. Huang, W.R. Tang, T.C. Wen, *J. Power Sources*, 164 (2007) 519.
57. C.W. Kuo, C.C. Yang, T.Y. Wu, *Int. J. Electrochem. Sci.*, 6 (2011) 3196.
58. Y. Hung, X. Duan, Y. Cui, L.J. Lauhon, K.H. Kim, C.M. Lieber, *Science*, 294 (2001) 1313.
59. J. Yano, H. Hirayama, Y. Harima, A. Kitani, *J. Electrochem. Soc.*, 157 (2010) B506.
60. C.W. Kuo, B.K. Chen, Y.H. Tseng, T.H. Hsieh, K.S. Ho, T.Y. Wu, H.R. Chen, *J. Taiwan Inst. Chem. Eng.*, 2012, in press, doi: 10.1016/j.jtice.2012.03.008.
61. Y.C. Zhao, L. Zhan, J.N. Tian, S.L. Nie, Z. Ning, *Electrochim. Acta*, 56 (2011) 1967.
62. M.W. Martínez, T.T. Thompson, M.A. Smit, *Int. J. Electrochem. Sci.*, 5 (2010) 931.

63. V. Selvaraj, M. Alagar, I. Hamerton, *Appl. Catal. B Environ.*, 73 (2007) 172.
64. Z. Qi, P.G. Pickup, *Chem. Commun.*, (1998) 2299.
65. J. Hwang, F. Amy, A. Kahn, *Org. Electron.*, 7 (2006) 387.
66. W. Deng, L. Yang, D. Fujita, H. Nejo, C. Bai, *Appl. Phys. A*, 71 (2000) 639.
67. S.K.M. Jonsson, W.R. Salaneck, M. Fahlman, *J. Mater. Res.*, 18 (2003) 1219.
68. V.D. Noto, E. Negro, *J. Power Sources*, 195 (2010) 638.
69. L. Qiu, B. Liu, Y. Peng, F. Yan, *Chem. Commun.*, 47 (2011) 2934.
70. W. Li, J. Lu, J. Du, D. Lu, H. Chen, H. Li, Y. Wu, *Electrochem. Commun.*, 7 (2005) 406.